

This figure "WRinM31.fig1a.jpg" is available in "jpg" format from:

<http://arxiv.org/ps/astro-ph/9907098v1>

This figure "WRinM31.fig1b1.jpg" is available in "jpg" format from:

<http://arxiv.org/ps/astro-ph/9907098v1>

This figure "WRinM31.fig1c.jpg" is available in "jpg" format from:

<http://arxiv.org/ps/astro-ph/9907098v1>

This figure "WRinM31.fig1d.jpg" is available in "jpg" format from:

<http://arxiv.org/ps/astro-ph/9907098v1>

TABLE 1. Physical properties of Group Ia shells.

Name ^a	Spec. type ^b	α (J2000)		δ (J2000)		Radius (pc)	L(H α) ^c ($\times 10^{36}$ ergs s ⁻¹)	Unresolved Excess H α emission	
		hh mm ss.ss		° ' "				L(H α) ($\times 10^{34}$ ergs s ⁻¹)	EW (Å)
ob135wr1	WNE	00 39 45.78		+40 23 02.9		60	23.8	13 \pm 5	35 \pm 3
MS11	WC4-5	00 40 22.47		+40 52 33.8		80	36		
ob69-F1	WC6-7	00 41 07.24		+41 04 16.9		25	12		
MS8	WCL	00 41 34.95		+41 05 51.6		30	7.5		
MS10	WC6	00 41 44.44		+40 45 15.8		55	19		
gwb1	WN	00 43 16.60		+41 45 15.3		75	39		
MS2	WC	00 43 41.61		+41 23 03.6		15	6.6		
IT1-40	WN	00 44 20.55		+41 54 11.7		50	5.8	3 \pm 1	21 \pm 4
ob54wr1	WN	00 44 37.56		+41 52 03.3		10	1.1		
IT5-2	WC	00 44 51.82		+41 29 06.3		15	3.9		
ob42wr2	WC6-7	00 45 01.07		+41 30 54.1		10	7.3		
ob48wr1	WN6-7	00 45 11.26		+41 38 14.9		70	9.2		
ob48wr6	WC6-7	00 45 10.36		+41 36 46.2		45	15	3 \pm 1	3 \pm 1
ob48wr3	WC	00 45 13.64		+41 37 42.3		60 ^d	24		
ob48wr2	WNE	00 45 14.07		+41 37 34.8		—	—	6 \pm 2	26 \pm 4
ob48-527	WN	00 45 17.56		+41 39 21.6		60	43	6 \pm 2	5 \pm 2
IT4-14	WC	00 45 51.26		+41 42 40.4		45	6.3		

^aWR star numbers and coordinates are from Massey & Johnson (1998), and references therein, except gwb1 where the information is taken from Galarza et al. (1999).

^bSpectral subtypes are from Massey & Johnson (1998), and references therein, except gwb1 where the information is taken from Galarza et al. (1999).

^cmultiply by 7.3×10^{11} to obtain Lyman continuum luminosity. Uncertainties ($\pm 0.1 \times 10^{36}$ ergs s⁻¹) don't include calibration errors, and systematic uncertainties due to varying the sizes and shapes of polygonal masks used to compute fluxes and background emission.

^dradius and luminosity for both ob48wr2&3

This figure "WRinM31.fig1b2.jpg" is available in "jpg" format from:

<http://arxiv.org/ps/astro-ph/9907098v1>

This figure "WRinM31.fig2a.jpg" is available in "jpg" format from:

<http://arxiv.org/ps/astro-ph/9907098v1>

This figure "WRinM31.fig2b.jpg" is available in "jpg" format from:

<http://arxiv.org/ps/astro-ph/9907098v1>

This figure "WRinM31.fig2c.jpg" is available in "jpg" format from:

<http://arxiv.org/ps/astro-ph/9907098v1>

TABLE 2. Physical properties of Group Ib shells.

Name ^a	Spec. type ^b	α (J2000)			δ (J2000)		Radius	L(H α) ^c	Unresolved Excess H α emission	
		hh	mm	ss.ss	°	' "			L(H α) ($\times 10^{34}$ ergs s ⁻¹)	EW (Å)
ob138wr1	WC	00	39	33.43	+40	20 18.4	$\frac{15}{40}$	6.3 28		
MS12	WC	00	40	19.46	+40	52 24.8	$\frac{10}{35}$	2.8 8.8		
MS14	WC	00	40	20.42	+40	48 07.7	$\frac{20}{80}$	4.8 4.2	7 \pm 1	245 \pm 100
MS6	WCL	00	42	14.38	+41	25 41.4	$\frac{10}{20}$	1.0 2.2		
MS4	WC7-8	00	43	31.08	+41	12 04.8	$\frac{10}{55}$	1.1 19		
ob10wr1	WC6-7	00	44	10.16	+41	32 52.4	$\frac{15}{35}$	1.9 5.2		
ob33wr3	WNL/Of	00	44	27.99	+41	21 00.2	$\frac{10}{20}$	1.6 4.7		

^aWR star numbers and coordinates are from Massey & Johnson (1998), and references therein.

^bSpectral subtype are from Massey & Johnson (1998), and references therein.

^cThe upper of the luminosity are for the inner shells, whereas the lower values are for the outer shell. Multiply by 7.3×10^{11} to obtain Lyman continuum luminosity. Uncertainties ($\pm 0.1 \times 10^{36}$ ergs s⁻¹) don't include calibration error and systematic uncertainties due to varying the sizes and shapes of polygonal masks used to compute fluxes and background emission.

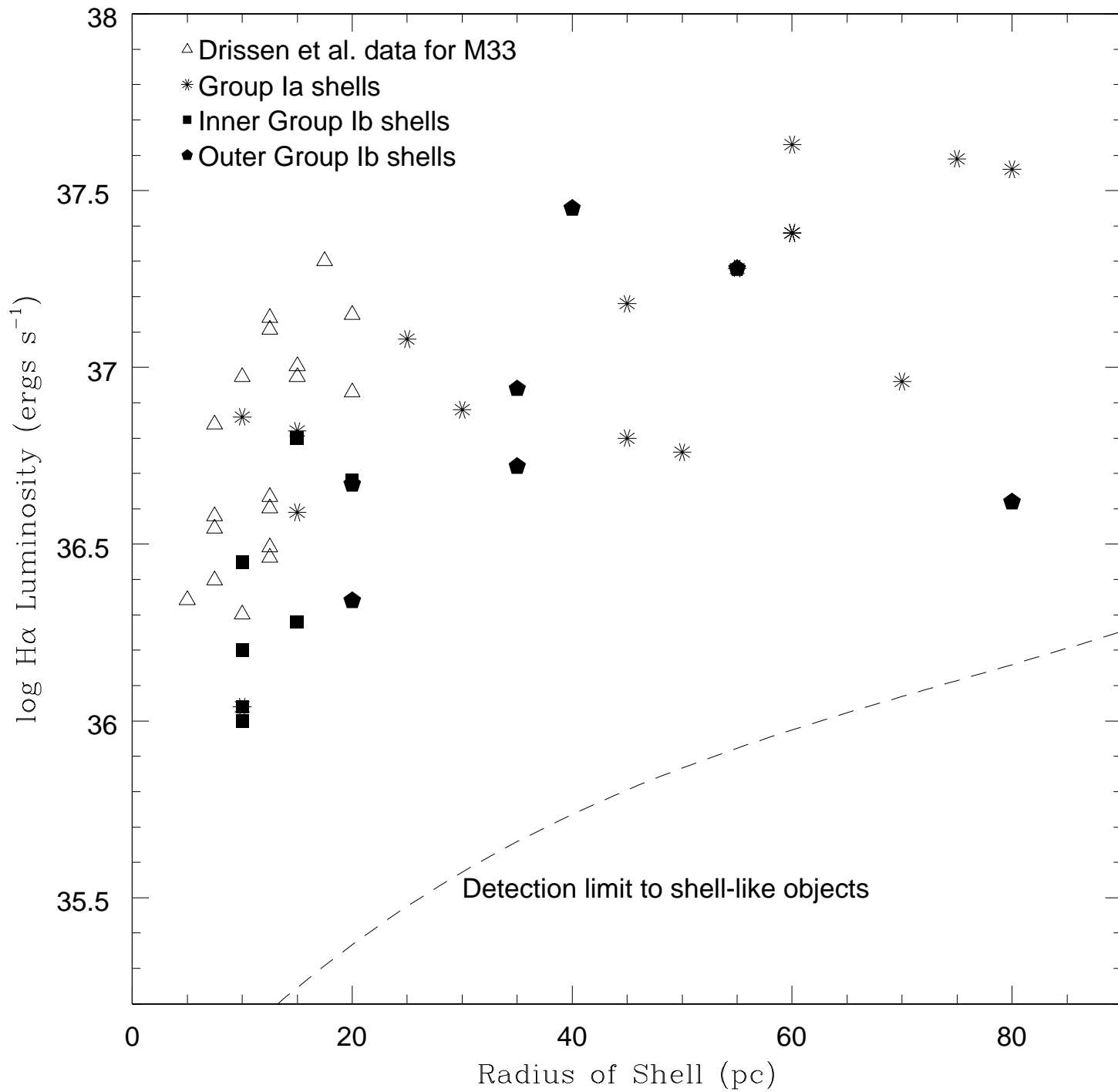
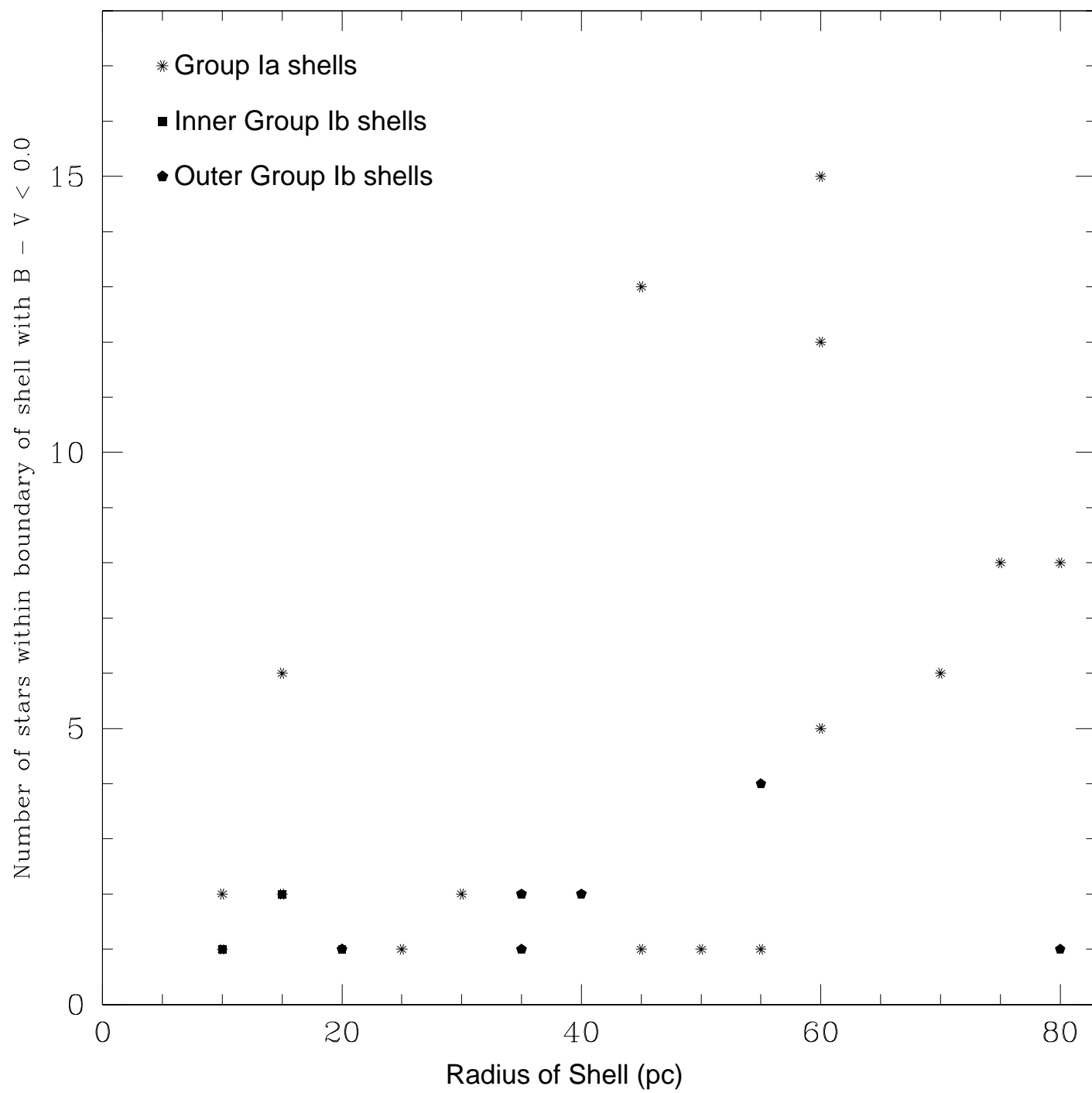


TABLE 3. Group IIa WR stars with unresolved excess H α emission.

Name ^a	Spec. type ^b	α (J2000) hh mm ss.ss	δ (J2000) ° ' "	L(H α) ($\times 10^{34}$ ergs s ⁻¹)	EW (Å)
ob136wr1	WN/C	00 39 19.50	+40 22 10.9	13 \pm 5	14 \pm 5
MS20	WN	00 40 21.01	+40 35 19.5	4 \pm 1	55 \pm 15
ob78wr5	WN/C	00 40 23.01	+40 44 54.3	6 \pm 1	18 \pm 4
ob78wr2	WNL	00 40 26.22	+40 44 59.6	10 \pm 2	26 \pm 4
IT5-15	WC6	00 44 12.39	+41 29 41.3	9 \pm 2	40 \pm 8
IT4-1	WC	00 45 24.12	+41 53 50.8	5 \pm 2	79 \pm 10

^aWR star numbers and coordinates are from Massey & Johnson (1998), and references therein.

^bSpectral subtype are from Massey & Johnson (1998), and references therein.



H II Shells Surrounding Wolf-Rayet stars in M31

M. A. Bransford, D. A. Thilker, R. A. M. Walterbos¹, and N. L. King¹

Department of Astronomy, New Mexico State University, Las Cruces, NM 88003

Received _____; accepted _____

arXiv:astro-ph/9907098v1 7 Jul 1999

¹Visiting Astronomer, Kitt Peak National Observatory, National Optical Astronomy Observatories, which is operated by the Association of Universities for Research in Astronomy (AURA) under cooperative agreement with the National Science Foundation.

ABSTRACT

We present the results of an ongoing investigation to provide a detailed view of the processes by which massive stars shape the surrounding interstellar medium (ISM), from pc to kpc scales. In this paper we have focused on studying the environments of Wolf-Rayet (WR) stars in M31 to find evidence for WR wind-ISM interactions, through imaging ionized hydrogen nebulae surrounding these stars.

We have conducted a systematic survey for H II shells surrounding 48 of the 49 known WR stars in M31. There are 17 WR stars surrounded by single shells, or shell fragments, 7 stars surrounded by concentric limb brightened shells, 20 stars where there is no clear physical association of the star with nearby H α emission, and 4 stars which lack nearby H α emission. For the 17+7 shells above, there are 12 which contain one or two massive stars (including a WR star) and that are ≤ 40 pc in radius. These 12 shells may be classical WR ejecta or wind-blown shells. Further, there may be excess H α point source emission associated with one of the 12 WR stars surrounded by putative ejecta or wind-blown shells. There is also evidence for excess point source emission associated with 11 other WR stars. The excess emission may arise from unresolved circumstellar shells, or within the extended outer envelopes of the stars themselves.

In a few cases we find clear morphological evidence for WR shells interacting with each other. In several H α images we see WR winds disrupting, or punching through, the walls of limb-brightened H II shells.

Subject headings: galaxies: individual (M31) — Local Group — stars: Wolf-Rayet — stars: mass loss (ring nebulae) — ISM: bubbles

1. INTRODUCTION

Wolf-Rayet (WR) stars are thought to be evolved, massive stars which have lost a significant fraction of their outer envelopes. They are sometimes surrounded by ring nebulae produced via the interaction of the central star with its stellar ejecta or surrounding ambient medium (e.g. Miller & Chu 1993). Studies of the chemistry, morphology and kinematics of Galactic WR ring nebulae have resulted in three main categories (e.g. Chu 1981): (a) radiatively excited H II regions (R-type); (b) stellar ejecta (E-type); (c) and wind-blown bubbles (W-type). A WR star does not play a primary role in the formation or shape of an R-type shell (generally $> 30\text{-}40$ pc in radius), only in its ionization. An E-type shell is produced when the WR stellar wind sweeps up mass lost from the star at an earlier epoch. Ejecta shells tend to be small ($\sim 5\text{-}10$ pc in radius; Chu 1981; Marston 1997), and are generally identified chemically by high nitrogen-to-oxygen ratios (indicative of CNO processing). The W-type shells ($\sim 10\text{-}20$ pc in radius) are produced when a strong WR stellar wind sweeps up ambient interstellar medium. Some Galactic WR stars have been observed to exist within H I shells (Arnal 1992). Eventually WR stars undergo a supernova explosion at the end of their lives. WR stars, therefore, have a substantial impact on their surroundings during the various phases of their evolution.

We present the results of an ongoing study focusing on the interaction of massive stars with the ISM, in nearby galaxies, from single stars to associations (see Thilker, Braun, & Walterbos 1998). Together, these investigations provide a detailed view of the processes by which massive stars shape the surrounding ISM, from pc to kpc scales. The main goal of this paper is to study the environments of WR stars to find evidence for WR wind-ISM interactions in M31, through imaging ionized hydrogen nebulae surrounding these stars.

We have conducted a systematic search for H II nebulae near WR stars in M31. Our results are based on new and previously published $H\alpha$, $H\alpha + [\text{N II}]$, and $[\text{S II}]$ imaging data

of M31 obtained at Kitt Peak National Observatory. M31 is attractive for this type of study due its proximity (nebulae are resolvable down to radii of ~ 7 pc) and the fact that it provides a uniform sample of WR stars at a well known distance (690 kpc). Surveys for WR stars in M31, while not complete, have resulted in a catalog of 48 WR stars (Massey & Johnson 1998). Another WR star has recently been discovered by Galarza, Walterbos, & Braun (1999).

We present $H\alpha$ and B images of the 48 of these 49 WR stars which fell within the area we imaged, and compile a catalog of ionized hydrogen nebular “shells” in their vicinity. Deciding when an H II shell is physically associated with a WR star (i.e. an E- or W-type shell) is not easy, since most WR stars are located close to other massive stars and near classical H II regions. Given the small size of Galactic E-shells we can barely resolve the larger shells of this type, but can easily resolve W- and R-type shells. Although we cannot distinguish W- and R-type shells based solely on imaging data, we attempt to determine which H II shells may be physically associated with WR stars based on criteria discussed below. Excess point source $H\alpha$ emission associated with WR stars might indicate unresolved E- or W-shells, or emission from a WR stellar wind. The Galactic WNL star HDE 313846 has a broad $H\alpha$ emission line, with an equivalent width of 23 \AA , which has been interpreted as arising in an extended outer envelope indicating a strong stellar wind (Crowther & Bohannan 1997). For this reason we also list the stars with unresolved $H\alpha$ excess.

The paper is organized as follows. In §2 and 3 we present details of the observations and data reduction. In §4 we describe our morphological classification of $H\alpha$ emission near WR stars, present $H\alpha$ and B images, and provide the physical properties of all detected H II shells. Further, we attempt to determine which shells are causally associated with a WR star. We discuss the environments of WR stars, and evidence for WR wind-ISM

interactions, in §5. We present our summary and conclusions in §6.

2. THE OBSERVATIONS

The data relevant to this study include previously published and new imaging data of M31, both obtained at the KPNO 0.9-m telescope. The earlier data were originally presented by Walterbos & Braun (1992; hereafter WB92). The WB92 data consist of 19 fields, located in the NE half of M31, imaged through 27 Å H α and [S II] filters, 75 Å off-band continuum and broad-band B. Each field measured $6'.7 \times 6'.7$. Further details may be found in WB92.

The new data, covering 8 fields mostly on the SW side of M31, were obtained during the nights of 4-10 November 1997. The fields were imaged through a pair of 75 Å H α + [N II] and off-band, red-shifted H α filters having nearly identical bandpass shape, in addition to a blue (B-band) filter. A 75 Å filter had to be used since narrower filters were not available to cover the radial velocities on the SW side of M31. Three to 7 individual frames were obtained for each H α + [N II], off-band, and B-band field. Total co-added exposure times for each H α + [N II] and off-band field ranged from 2400 to 5400 s, and for the B-band fields from 180 to 690 s.

The images were obtained using a TI $2k \times 2k$ CCD detector. Individual pixels measure $24 \mu\text{m}$, which corresponds to $0''.68$ or 2.3 pc at the distance of M31 (690 kpc). The fields measure $23'.2$ on a side or, ignoring projection effects due to inclination, $4.6 \times 4.6 \text{ kpc}^2$. The typical resolution of the WB92 data set was $2''$, and for the 1997 data set $\sim 1\text{--}2''$ (which corresponds to a linear resolution of $\sim 4\text{--}7 \text{ pc}$). Future papers will provide the entire 1997 data set and its reduction, although we outline some essential reduction details here.

3. DATA REDUCTION AND CALIBRATION OF 1997 DATA SET

Initial reduction of the individual frames (bias subtraction and flat fielding) was performed within IRAF². A twilight “master-flat” was constructed by co-adding twilight flats from several different nights, in each filter. The twilight master-flats successfully removed sensitivity variations across the chip. This could be seen by the uniformity of the dome flats after correcting them with the master-flats. Residual, large-scale variations were of the order 1% across the field. Registered H α + [N II], off-band, and blue images were then combined and cosmic rays were removed, using the IRAF routine IMCOMBINE. The continuum images were scaled to foreground stars in the H α + [N II]+continuum images, and then subtracted to produce line emission images. The images presented in this paper are each displayed with a logarithmic scaling, to emphasize faint emission and structure within the H α emission.

The line images were flux calibrated using the Oke & Gunn (1983) standard star HD 19445. We corrected for the slight effect of H α absorption in the standard star. The rms noise after calibration and continuum subtraction is $\sim 2 \times 10^{-17}$ ergs s⁻¹ cm⁻² pix⁻¹. Expressed in emission measure (the integral of the electron density *squared* along the line of sight) this corresponds to 22 pc cm⁻⁶, assuming an electron temperature of 10,000 K (note that for ionized gas at 10,000 K, 5.6×10^{-18} erg s⁻¹ cm⁻² arcsec⁻² = 2.8 pc cm⁻⁶ (e.g. WB92)). The accuracy of the calibration was tested by comparing the fluxes of several normal H II regions in overlapping fields between the 1997 data set and WB92. The fluxes in the 1997 data are higher by $\sim 30\%$. Since the WB92 data did not contain emission from

²IRAF (Image Reduction and Analysis Facility) is provided by the National Optical Astronomy Observatories (NOAO). NOAO is operated by the Association of Universities for Research in Astronomy (AURA), Inc. under cooperative agreement with the National Science Foundation

the [N II] $\lambda\lambda$ 6548,6584 lines, and the ratio of [N II]/H α intensities was assumed to be 0.3 in WB92, agreement between the data sets is satisfactory.

In order to easily locate the positions of WR stars within our images, the absolute orientation of the fields was determined using an astrometry routine within IDL. This program was interactively given the (X,Y) coordinates of several HST guide stars within our fields. The known (α,δ) coordinates of the guide stars were then used to determine a plate scale solution, giving each frame a positional accuracy of $\sim 1''$ relative to the guide star reference frame.

4. IDENTIFICATION AND PHYSICAL OF PROPERTIES OF H II SHELLS

We have classified the morphology of H α emission near WR stars into two groups. The first category (Group I shells) consists of H II shells, or shell fragments, in which the WR star is at or near the center of a single shell (Ia), or concentric limb brightened shells (Ib). We consider Group I shells as potentially being causally associated with a WR star. Note that the multiple shells presented here are probably not physically related to the multiple shells reported by Marston (1995), since the former are generally E-type shells, which are barely resolved in our data. The second category (Group II stars) consists of WR stars where there is no clear causal relation with nearby H α emission (IIa), or a lack of nearby H α emission (IIb). Group IIa consists of WR stars that are either near amorphous, diffuse H α emission, or on the edge of H II regions, and therefore have no preferred location with respect to an H II shell. There are 17 WR stars surrounded by Group Ia shells, 7 stars surrounded by Group Ib shells, 20 Group IIa stars, and 4 Group IIb stars.

H α fluxes were computed for Group I shells, but not for nebular emission near Group II stars. Polygonal masks (shown in Figure 1, see below) used to compute the fluxes were

chosen such that they most likely contain all emission from a given H II shell. Regions for Group Ia shells are generally circular or elliptical in shape. The multiple polygons for Group Ib shells are concentric in nature. The interior polygons defined for Group Ib shells are used to compute the fluxes of the inner shells, and the outer polygons are used to compute the fluxes of the inner+outer shells. Outer shell fluxes then are obtained as the difference of these two measurements. We defined irregularly shaped regions for shell fragments, such that the boundary traced the H α emission associated with a fragment. Masks containing shell fragments therefore tend to be arc shaped. Pixels within the regions defined above were summed to produce the total shell+background fluxes. The background was estimated from one or more polygonal regions immediately surrounding an H II shell (not shown), and were generally 2-3 times larger in area than the regions used to compute the shell+background fluxes. The background was then subtracted to produce a total shell H α flux. Uncertainties in the flux were estimated by adding in quadrature the rms background uncertainty, for the number of source pixels, and root-N photon noise.

The sizes of shells were estimated by measuring several (5-10) radial distances from a WR star to the outer edge of its surrounding shell, and averaging these values. For a given H II shell, the uncertainties in the measurements varied depending on factors such as the completeness and/or ellipticity of the shell. Radii were rounded to the nearest 5 pc, and have typical uncertainties of ± 5 pc.

Figure 1a contains H α + [N II] and blue (B-band) images of Group Ia shells from the 1997 data set. The regions used to compute the H II shell fluxes are indicated. The B images serve as finder charts and illustrate the spatial distribution of surrounding luminous stars. Figure 1b is the same as Figure 1a, but contains images of Group Ia shells from WB92. The H α images lack contribution from [N II] $\lambda\lambda 6548, 6584$ emission in this case. Group Ib shells are shown in Figure 1c from the 1997 data set and in Figure 1d from

WB92. We note that the Group Ia shell surrounding MS11 appears in Figure 1c, due to its proximity with MS12, which is surrounded by a Group Ib shell. The names of the WR star(s) appearing in the images are written above the blue images. The central WR star name appears first whenever there is more than one WR star per image. Tables 1 & 2 contain a listing of the properties of the H II shells presented in Figure 1, including the spectral subtype of the central star and its coordinates, radii of the shells, and integrated H α luminosities (uncorrected for possible extinction).

Images of Group IIa stars are shown in Figure 2a, from the 1997 data set, and Figure 2b, from WB92. Due to the proximity of ob33wr3 and ob33wr2, the latter is shown in Figure 1c, although we consider this star to belong to Group IIa. Group IIb stars are shown in Figure 2c, from the 1997 data set.

The H α luminosity of Group I H II shells, presented in Figure 1, ranges between 1 and 43×10^{36} ergs s $^{-1}$. In Figure 3 we show the distribution of H α luminosities as a function of the size of the nebulae, and plot the same distribution for the nebular structures surrounding WR stars in M33 (data from Drissen, Shara, & Moffat 1991). Further we indicate the detection limit in our data, with regard to shell-like objects. The minimum detectable luminosity for shells of varied size was determined empirically through the use of a simple code for modeling the anticipated appearance of idealized bubbles in a noisy background. Our program initially computes the projected surface brightness distribution of a shell (at very high spatial resolution) then transforms to an observable form by convolving with an appropriate Gaussian PSF and regridding. Finally, we scale the simulated image to units of emission measure. This result is added to a realistic noise background matching the properties of our observations. Inspection of the shell image with noise added determines whether or not a source of the specified size and luminosity would be detected in our survey. Although rather conservative, this procedure does not reflect non-detection associated with

confusion due to neighboring emission line sources. We suspect that the ambiguity related to objects bordering the WR star may often dominate the “error budget” for non-detection of WR shells. For this reason, the detection limit indicated in Figure 3 should be interpreted as a best-case scenario, appropriate when the WR star is relatively isolated but otherwise just a lower limit.

Figure 3 reveals that there is a gap between the detection limit and the $H\alpha$ emission from Group I shells. Why don’t we detect fainter shells? One possible explanation is that the larger shells are R-type, with many massive stars responsible for their ionization. Typically Galactic WR shells expand at $10\text{--}50 \text{ km s}^{-1}$ (Marston 1995), therefore a shell would need $\geq 4 \times 10^5$ years to expand to a radius of 20 pc. If the WR phase lasts $10^4\text{--}10^5$ years (Marston 1995) shells larger than 20 pc would no longer contain a WR star. The problem with this explanation is that these timescales hold true only if the shell were to begin expanding from the surface of the star. Shells, however, are likely to form far from the surface of the star. In the intervening space between the star and the radius at which the shell is formed, the stellar wind (or possible ejecta) may expand at a much higher velocity than the observed expansion velocity of the resulting shell. Further, one must consider mass loss from pre-WR phases. The winds of massive stars can operate on timescales of several Myr (the typical lifetime of an O star), affecting the ISM up to radii of tens of parsecs. As for the gap at small shell radii, there may be unresolved circumstellar shells ($\leq 5\text{--}7$ pc) surrounding WR stars in our data (see below). The point source detection limit is $\log L_{H\alpha} \sim 34.5$, well below the scale in Figure 3. We note that the upper limit of possible shell emission surrounding Group IIb stars also falls below this scale. The gap therefore remains somewhat surprising.

The implied Lyman continuum luminosity of Group I shells ranges from 0.8 to 31.8×10^{48} photons s^{-1} . Esteban et al. (1993) have estimated that Galactic WR stars can supply

4 to 37×10^{48} photons s^{-1} , indicating that all Group I shells can in principle be ionized by a single WR star. However, this is not proof that the only source of ionization is the WR star. Spectral classification of the brightest blue stars within the projected boundaries of the nebulae would be necessary to convincingly resolve this issue.

We now discuss which Group I shells may be physically associated with a solitary WR star. Our criteria are based on (a) the number of nearby massive stars (other than the WR star), and (b) a comparison of the sizes of the Group I shells with the sizes of WR nebulae in the LMC.

In Figure 4 we plot the sizes of Group I shells versus the number of nearby, potentially ionizing stars (including the WR star in all cases). Stars were selected if they were both (a) within one shell radius (and therefore within the boundary of the shell or shell fragment), and (b) have $B - V$ colors ≤ 0 (photometry is taken from Magnier et al. (1992)). Only stars bluer than B0 ($B - V = -0.3$) can supply enough ionizing photons to be consistent with the $\text{H}\alpha$ luminosities of Group I shells. Our choice of $B - V \leq 0$ was prompted by considering the following two factors. First, there are substantial uncertainties in the photometry from the Magnier catalog. Second, we have made no reddening corrections. Thus the color information on stars in the field is, unfortunately, crude. Note in Figure 4 that Group I shells with radii less than ~ 40 pc generally contain one or two ionizing stars.

Rosado (1986) reported the radii of shells associated with (a) single WR stars, (b) single OB stars, and (c) multiple OB & WR stars in the LMC. The mean radii are, respectively, 15 ± 7 pc, 27 ± 4 pc, and 69 ± 33 pc (Rosado 1986). Single massive stars in the LMC are surrounded by shells up to ~ 30 pc in radius, consistent with the radius estimated above for Group I shells

We suggest, allowing for chance alignment, those shells containing one or two ionizing stars (including a WR star), or that are ≤ 40 pc in radius, are possibly of E- or W-type.

There are 5 Group Ia shells that satisfy this criteria: ob69-F1, MS8, MS2, ob54wr1, and ob42wr1. All 7 inner Group Ib shells satisfy this criteria, although the outer shells for MS14 and MS4 do not. Therefore, 12 of the 48 WR stars we observe (25%) may be surrounded by “classical” WR E- or W-type shells. The remaining 11 Group Ia shells contain three or more stars, or have a radii >40 pc, and are probably R-type.

Previous observations have suggested Galactic E- and W-type shells are generally <20 pc in radius (Chu 1981; Marston 1997). Our data (in particular see Figure 4), on the other hand, suggest that the H II shells of this type *may* be larger in M31, on average, than their Galactic counterparts. However, some of our larger shells (including those classified as R-type) may be (and in some instances probably are) classical, ring-like H II regions or, for the very largest shells, “superbubbles” (e.g. Oey & Massey 1994; Oey 1996), and may not be “classical” WR ring nebulae. Future observations to specifically classify the H II shells presented in this paper, as either E-, W- or R-type, would be necessary to verify that E- or W-shells are indeed larger in M31 than the Galaxy.

WR ring nebulae in the Galaxy and LMC have revealed interesting statistical trends, suggesting WC stars generally are found within nebulae of larger size than WN stars (Miller & Chu 1993; Marston 1997; Dopita et al. 1994), possibly indicating an evolutionary sequence. We compared the size distribution of the H II shells surrounding WN stars with those surrounding WC stars in M31. In light of the discussion above, we restricted our comparison to shells ≤ 40 pc in radius, and containing one or two massive stars (i.e. those shells thought to be causally related to a single WR star). For this particular subset of shells (3 contain WN stars and 14 contain WC stars) we found that shells containing a WN star were on average smaller than those containing a WC star. If true, this supports the evolutionary sequence, $WN \rightarrow WC$ (Marston 1997). However, given the small number of shells (in particular those containing WN stars), our result is not statistically significant.

Further, considering all H II shells in our sample, there are as many WN stars within small shells (putative E- or W-type) as big shells (putative R-type), as can be seen from Tables 1 & 2. We therefore caution that this result should be viewed as preliminary.

We conclude this section by discussing the excess point source H α emission associated with a subset of WR stars in the 1997 and WB92 data. There are 12 stars with possible excess emission in the H α passband. Tables 1 & 2 list the luminosities and equivalent widths of the excess emission for those WR stars within Group I shells, and Table 3 for those stars in Group IIa. No stars within Group IIb have excess emission. Excess H α emission associated with WR stars might indicate unresolved E- or W-shells, or emission from a WR stellar wind. We note that a small contribution from stellar He II $\lambda 6562$ may also be present in the H α passband, but not enough to explain the equivalent widths of the excess emission. The luminosities of the excess emission range from 3 to 10×10^{34} ergs s $^{-1}$, the equivalent widths from 5 to 240 Å. By way of comparison, the Galactic stellar ejecta nebula RCW 58 has an H α luminosity of 1×10^{35} ergs s $^{-1}$ (Drissen et al. 1991), and WNL 313846 has a broad H α emission line, with an equivalent width of 23 Å, interpreted as arising in an extended outer envelop and indicative of a strong stellar wind (Crowther & Bohannon 1997). Crowther & Smith (1997) find that four LMC WN9-11 stars show nebular H α emission lines (equivalent widths ranging from 32 to 83 Å) superimposed on their stellar spectra, which is circumstellar and not from an underlying H II region.

5. WR WIND-ISM INTERACTIONS

Figure 1c contains an image of the Group Ia shell surrounding MS11 and the Group Ib shell surrounding MS12. The bright star near the top of the B-band image is a foreground star. MS11 is off-set from the center of a large, limb-brightened bubble, and is part of a chain of OB stars. To the south-west of MS11 is a multiple shell surrounding the WR star

MS12. MS12 is at the center of a small inner shell, and offset to the west from the center of the outer shell. MS12 is the only nearby ionizing star, which is supported by the flux of ionizing photons implied by the $H\alpha$ luminosity of the surrounding shells.

Interestingly, there is morphological evidence that the shells surrounding these stars may be interacting. Pointing radially away from MS11 is a faint loop of $H\alpha$ emission. Perhaps not coincidentally, the outer shell surrounding MS12 appears to be impinging on the shell surrounding MS11, directly south of the $H\alpha$ loop (or “break-out” feature), causing a noticeable s-shaped distortion in the surface of the larger shell. The $H\alpha$ emission in the limb of the Group I shell is clearly enhanced in the region to the north and south of the $H\alpha$ loop. An effect of the expansion of these shells into one another may have been to weaken the surface of the Group I shell, such that the fast wind from MS11 was able to punch a hole in its wall. Interestingly, there is a gap between the shells. Therefore, if the shells are interacting this would imply they are radiation bounded, and the outer layers of the shells are likely neutral.

In Figure 1d we see, for ob33wr3 and ob33wr2, another interesting case of potentially interacting shells, and the effects of WR winds. A large arc of emission south-west of ob33wr3 is impinging upon a shell structure containing ob33wr2. Interestingly, the Group Ib shell is centered within this arc. As above, the gap between the shell and this arc could indicate the shell is radiation bounded, with neutral material in between. The possibility of a neutral outer layer is strengthened by the evidence for a dust lane, seen in the B image, superimposed on the gap. The probable action of a fast wind arising from ob33wr2 is evident from a small cavity (blown?) in the wall this shell, south-east of the star. An arc is seen surrounding ob10wr1 (see Figure 1d) perhaps being driven into ob10 by the expansion of this Group Ib shell. Finally, the potential action of a WR wind can be seen for the case of the Group IIa star MS17 (see Figure 2a), where it has apparently disrupted the wall of a

diamond shaped H II shell, in which it is embedded.

Obtaining detailed kinematics (in both the ionized and neutral gas) of these interacting shells, and the gas effected by WR winds, may prove extremely useful in understanding the dynamical evolution of shell structures in the ISM of galaxies. Further, in addition to spectroscopy, narrow-band imaging, in lines such as [O III] λ 5007 or [O I] λ 6300, may prove useful in detecting shock fronts in a wind-ISM interaction region. Will shells merge to become larger single structures? What role do WR winds play in enlarging pre-existing shell structures? Are the shells, presented in this paper, the evolutionary precursors of H I shells (or supershells). What role do WR stars play in producing a frothy H I medium in galaxies?

6. SUMMARY AND CONCLUSIONS

We have presented the results of an ongoing investigation to provide a detailed view of the processes by which massive stars shape the surrounding ISM, from pc to kpc scales. In this paper we have focused on studying the environments of WR stars to find evidence for WR wind-ISM interactions in M31, through imaging ionized hydrogen nebulae surrounding these stars.

We have classified the morphology of the H α emission near 48 WR stars into two groups, Group I and Group II. The first category (Group I shells) consists of H II shells, or shell fragments, in which the WR star is at or near the center of a single shell (Ia), or concentric limb brightened shells (Ib). We consider Group I shells as potentially being causally associated with a WR star (i.e. E- or W-type shells). There are 17 WR stars within Group Ia shells, and 7 stars within Group Ib shells. The second category (Group II stars) consists of WR stars where there is no clear causal relation with nearby H α emission

(IIa), or a lack of nearby $H\alpha$ emission (IIb). Group IIa consists of WR stars that are either near amorphous, diffuse $H\alpha$ emission, or on the edge of H II regions, and therefore have no preferred location with respect to an H II shell. There are 20 Group IIa stars, and 4 Group IIb stars. Of the 48 WR stars in our sample, 24 are surrounded by Group I shells (50%) and 24 are Group II stars (50%).

We suspect that Group I shells which contain one or two massive stars, or are ≤ 40 pc in radius, may be E- or W-type shells. There are 5 Group Ia shells that satisfy this criteria: ob69-F1, MS8, MS2, ob54wr1, and ob42wr1. All 7 inner Group Ib shells satisfy these criteria, although the outer shells for MS14 and MS4 do not. Therefore, 12 of the 24 WR stars within Group I shells (or 25% of the sample of 48) appear surrounded by resolved E- or W-type shells.

There are 12 WR stars (25% of the sample) that have excess emission within the $H\alpha$ bandpass (one WR star with excess emission is in common with the 12 WR stars surrounded by putative E- or W-type shells). The excess $H\alpha$ emission may arise from unresolved E- or W-type shells, or in an extended outer envelope indicating a strong stellar wind. Excess unresolved emission occurs for stars within Group I shells, and for Group IIa stars. No stars within Group IIb have excess emission. If we assume that the unresolved excess $H\alpha$ emission arises from an unresolved E- or W-type shell, nearly one-half of our sample may have surrounding E- or W-type shells.

We find morphological evidence that shells surrounding MS11 and MS12, and ob33wr3 and ob33wr2, may be interacting. Interestingly, there are gaps between the shells. Therefore, if these shells are interacting this implies they are radiation bounded, and the outer layers of the shells are likely neutral. An arc is seen surrounding ob10wr1 perhaps being driven into ob10 by the expansion of this Group Ib shell. Obtaining detailed kinematics (in both the ionized and neutral gas) of these interacting shells, and the gas effected by WR winds,

may prove extremely useful in understanding the dynamical evolution of shell structures in the ISM of galaxies.

Acknowledgements

We would like to thank Phil Massey for a useful conversation when visiting NMSU. This research was partially supported by the National Science Foundation through grant AST 96-17014.

REFERENCES

- Arnal, E. M. 1992, A&A, 254, 305
- Chu, Y.-H. 1981 ApJ, 249, 195
- Crowther, P. A., & Bohannon, B. 1997, A&A, 317, 532
- Crowther, P. A., & Smith, L. J. 1997, A&A, 320, 500
- Dopita, M. A., Bell, J. F., Chu, Y.-H., & Lozinskaya, T. A. 1994, ApJS, 93, 455
- Drissen, L., Shara, M. M., & Moffat, A. F. J. 1991, AJ, 101, 1659
- Esteban, C., Smith, L. J., Vilchez., J. M., & Clegg, R. E. S. 1993, A&A, 272, 299
- Galarza, V., Walterbos, R. A. M., & Braun, R. 1999, ApJ, submitted
- Magnier, E. A., Lewin W. H. G., van Paradijs J., Hasinger G., Jain A., Pietsch W.,
Truemper J. 1992, A&AS, 96, 379
- Marston, A. P. 1997, ApJ, 475, 188
- Marston, A. P. 1995, AJ, 109, 1839
- Massey, P., & Johnson, O. 1998, ApJ, 505, 793
- Miller, G. J., & Chu, Y.-H. 1993, ApJS, 85, 137
- Oey, M. S. 1996 ApJ, 467, 666
- Oey, M. S., & Massey, P. 1994 ApJ, 425, 635
- Oke J. B., & Gunn J. E. 1983, ApJ, 266, 713
- Rosado, M. 1986, A&A, 160, 211

Thilker, D., Braun, R., & Walterbos, R. A. M. 1998, A&A, 332, 429

Walterbos, R. A. M., & Braun, R. 1992, A&AS, 92, 625 (WB92)

Fig. 1a.— $H\alpha$ + $[N\ II]$ and blue (B-band) images of Group Ia shells from the 1997 data set. The regions used to compute the H II shell fluxes are indicated. The B images serve as finder charts and illustrate the spatial distribution of surrounding luminous stars. The names of the WR star(s) appearing in the images are written above the blue images. The central WR star name appears first whenever there is more than one WR star per image. The images measure $300 \times 300\ \text{pc}^2$.

Fig. 1b.— Same as Figure 1a, but contains images of Group Ia shells from WB92. The $H\alpha$ images lack contribution from $[N\ II]\lambda\lambda 6548, 6584$ emission in this case.

Fig. 1c.— Same as Figure 1a, but shows Group Ib shells from the 1997 data set.

Fig. 1d.— Same as Figure 1b, but shows Group Ib shells from WB92.

Fig. 2a.— Images of Group IIa stars from 1997 data set.

Fig. 2b.— Images of Group IIa stars from WB92.

Fig. 2c.— Images of Group IIb stars from 1997 data set.

Fig. 3.— Distribution of $H\alpha$ luminosities as a function of the size of the nebulae. Also shown is the same distribution for the nebular structures surrounding WR stars in M33 (data from Drissen, Shara, & Moffat 1991). Further we indicate the detection limit in our data, with regard to shell-like objects.

Fig. 4.— Radii of Group I shells versus the number of nearby, potentially ionizing stars (including the WR star in all cases).